RESEARCH PAPER

Design, Synthesis, and Biological Evaluation of Ortho- and Meta-Phenyl-Substituted Pyrrolo[2,1-f][1,2,4]triazine Derivatives as Novel Phosphoinositide 3-Kinase *α* Inhibitors

Sagar Patni[1], Ajay Kumar[1*], Snehil Singh[1], Shashi Kiran Misra[1]

[1]School of Pharmaceutical Sciences, Chhatrapati Shahu Ji Maharaj University, Kanpur, Uttar Pradesh, 208024 *India*

Email: patnisagar1@gmail.com, ajaykumar@csjmu.ac.in, patnisnehil1@gmail.com, shashikmishra@csjmu.ac.in

ABSTRACT

The phosphoinositide-3-kinase-α is a key regulator of tumor progression across different cancers, including breast cancer. Herein, we explored a novel series of PI3K-α (Phosphatidylinositol-3-kinases alpha subunit) inhibitors with the structure of pyrrolo[2,1-f][1,2,4]triazine scaffold have been designed and synthesized. Structure-guided drug design and lead optimization efforts led to the identification of dioxido-thiomorpholine analog as a PI3K-α inhibitor, which ffectively inhibits the growth of MDA-MB-231 cells by targeting p110α, PI3K/AKT/mTOR (Mammalian target of rapamycin) pathways, enhancing the expression of apoptotic proteins and impeding the cell's migratory capabilities. Compound 4-(2-(3-aminophenyl)pyrrolo[2,1-f][1,2,4]triazin-4-yl)thiomorpholine 1,1-dioxide (10l) occupies the PI3K-α hinge pocket and forms H-bonding with VAL851, as well as with GLN859, a nonconserved residue linked to isoform selectivity. Docking studies indicate the dioxido-thiomorpholine group in 2-position of pyrrolo[2,1-f][1,2,4]triazine is necessary for the potent antitumor activity, which confirms our design is reasonable.

Keywords: PI3K inhibitors, PI3K/Akt/mTOR pathway, Molecular docking, Physicochemical Profiling

How to cite this article: Patni S, Kumar A, Singh S, Misra S. K., Design, Synthesis, and Biological Evaluation of Ortho- and Meta-Phenyl-Substituted Pyrrolo[2,1-f][1,2,4]triazine Derivatives as Novel Phosphoinositide 3-Kinase α Inhibitors. Int J Drug Deliv Technol. 2026;16(38): 08-33.

DOI: NA

Source of support: Nil

Conflict of interest: None

GRAPHICAL ABSTRACT

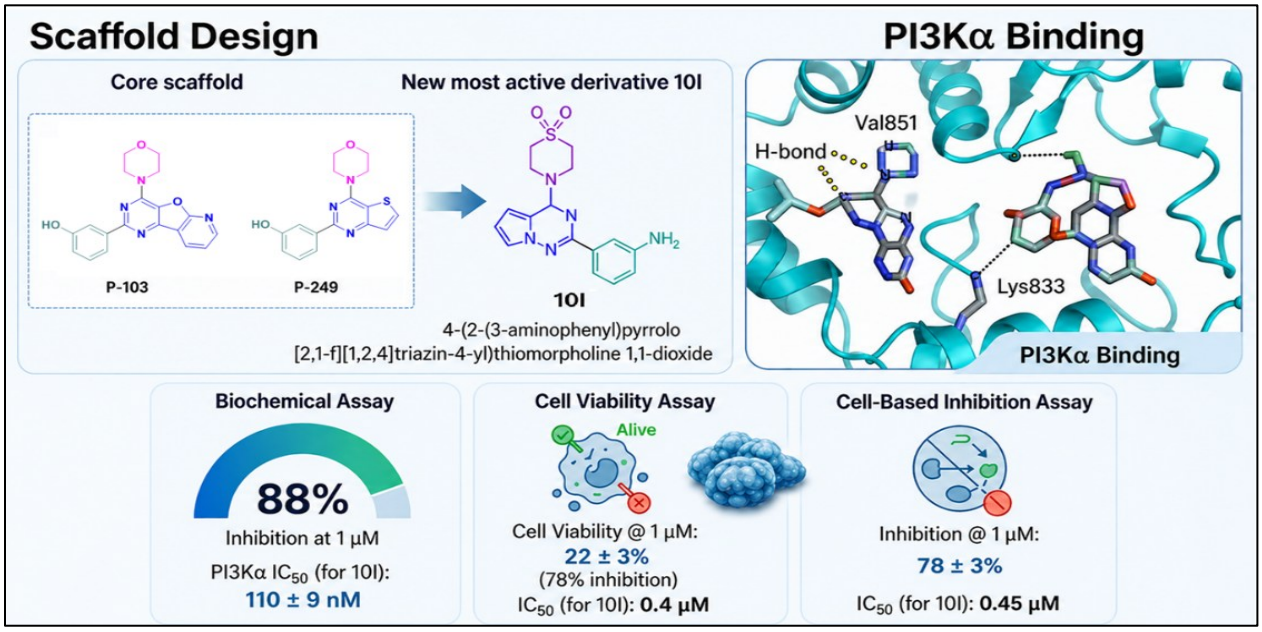

1.INTRODUCTION

Non-Phosphoinositide-3-Kinases (PI3Ks) constitute a key family of lipid kinases that regulate a variety of cellular processes, including cell growth, proliferation, metabolism, and survival. Dysregulation of the PI3K signalling cascade has been strongly associated with cancer initiation and progression, which has made this pathway an attractive target for the development of anticancer therapeutics. Among the four class I PI3K isoforms (α, β, γ, and δ), the PI3K-α isoform has received the greatest attention in oncology because activating mutations in this enzyme are frequently detected in a wide range of tumours. In contrast, the other isoforms have more specialised physiological roles; the β isoform is primarily involved in platelet activation and thrombus formation, whereas the δ and γ isoforms play critical roles in immune signalling, inflammatory responses, and autoimmune diseases.[1-3] Consequently, substantial efforts in medicinal chemistry have focused on the discovery of inhibitors that selectively target the PI3K-α isoform.[4]

Significant progress has been made in the development of therapeutics targeting the PI3K pathway. To date, five PI3K inhibitors have received regulatory approval from the U.S. Food and Drug Administration, including Idelalisib (1) for chronic lymphocytic leukaemia, Copanlisib (2) for lymphoma, Duvelisib (3) for chronic lymphocytic leukaemia, Alpelisib (4) for breast cancer, and Inavolisib (5) for breast cancer.[5-8] In addition to these approved agents, numerous PI3K inhibitors have been reported in both preclinical and clinical studies. Many of these compounds have served as valuable chemical tools in structure-based drug design, enzyme structural investigations, and as starting points for the development of more advanced therapeutic candidates.

Among these investigational compounds, Serabelisib (6) is a potent and orally bioavailable PI3K-α inhibitor originally discovered by Takeda Pharmaceutical Company. This compound is currently undergoing clinical evaluation for the treatment of triple-negative breast cancer (TNBC) by Petra Pharma and Faeth Therapeutics. [9-10] Another widely studied compound is PI-103 (7), a pyridofuropyrimidine-based inhibitor that has been extensively used as a preclinical tool compound. PI-103 exhibits potent inhibitory activity against all four class I PI3K isoforms (α, β, γ, and δ) as well as the related kinases mTORC1 and mTORC2, with reported IC_{50} values of 3.6, 3, 150, and 3 nM for PI3K-α, β, γ, and δ, respectively, and 20 and 83 nM for mTORC1 and mTORC2.[11]

Advances in structural biology have significantly facilitated the rational design of isoform-selective PI3K inhibitors. For example, the PI3K-α selective inhibitor GDC-0326, developed by Genentech, contains a terminal amide functionality capable of forming a hydrogen-bond interaction with residue GLN859 located within the PI3K-α active site. Structural analyses, particularly ligand-bound co-crystal studies, have demonstrated that residues HIS855 and GLN859 form a solvent-exposed region with a conformation that differs from those observed in other class I PI3K isoforms. This structural feature, particularly the presence of GLN859, offers a valuable opportunity for designing highly selective PI3K-α inhibitors.[12]

The thienopyrimidine derivative PI-249 (8) has also been reported as a potent inhibitor of the PI3K-α isoform[13-16] Although both PI-103 (7) and PI-249 (8) display strong in vitro inhibitory activity, their further development was restricted by unfavourable pharmacokinetic properties, particularly poor absorption, distribution, metabolism, and excretion (ADME) characteristics.[17]

Nevertheless, these molecules have proven highly valuable as chemical probes in numerous mechanistic studies and have served as key starting points for the development of clinically relevant inhibitors, including Pictilisib (GDC-0941), Compared with earlier PI3K inhibitors such as Wortmannin and LY294002, PI-103 exhibits greater potency, improved selectivity among PI3K isoforms, and enhanced chemical stability. Since its initial discovery, PI-103 has been widely employed as a pharmacological tool compound and has been cited in numerous studies investigating the PI3K signalling pathway.[18-20]

Preclinical investigations have shown that PI-103 achieves sufficient pharmacokinetic exposure in plasma and tumour tissues in mouse models, enabling proof-of-concept evaluation of its antitumor activity across several human tumour xenograft models. In addition to its direct antiproliferative activity, PI-103 has been reported to influence multiple biological processes associated with tumor progression, including cellular invasion, angiogenesis, and metastatic spread. These effects are primarily attributed to the induction of cell-cycle arrest at the G1 phase, accompanied by decreased cyclin D1 expression and increased levels of the cyclin-dependent kinase inhibitor p27.[21]

Subsequent optimisation of the thienopyrimidine scaffold has led to the discovery of several PI3K inhibitors that have progressed into clinical development. One such example is Pictilisib (GDC-0941, 9), which has been evaluated in multiple Phase I and Phase II clinical studies conducted by Genentech.[22-24] Another compound derived from this research program is GDC-0326 (10), an isoform-selective PI3K-α inhibitor that has advanced into clinical trials.[10] In addition, Gedatolisib (11) is a highly potent dual PI3K/mTOR inhibitor capable of simultaneously targeting all class I PI3K isoforms as well as the mTORC1 and mTORC2 complexes, displaying sub-nanomolar to low-nanomolar inhibitory activity against

Corresponding Author: Dr. Ajay Kumar, ajaykumar@csjmu.ac.in

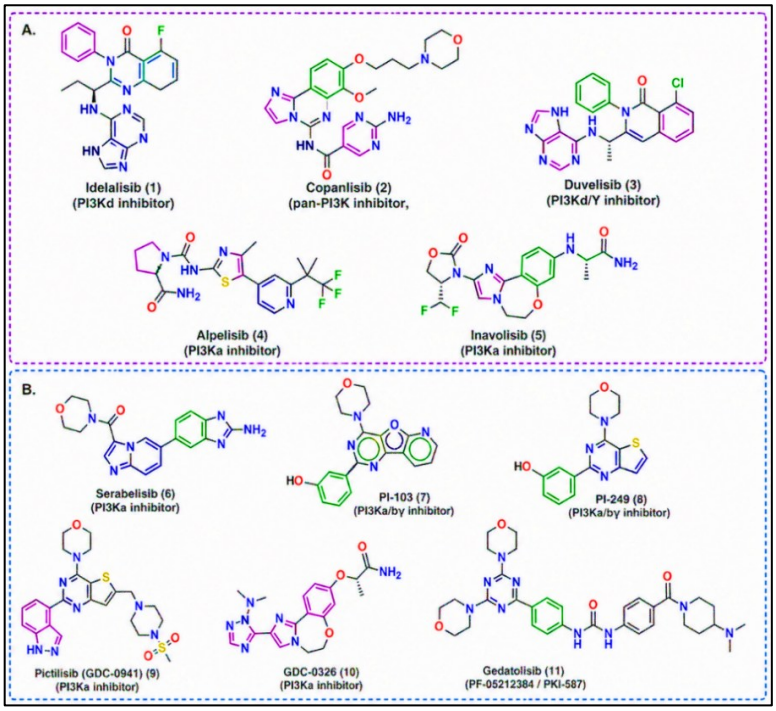

Figure 1. Chemical structures of PI3K inhibitors. **(A).** FDA-approved PI3K inhibitors, viz., idelalisib, copanlisib, duvelisib, alpelisib, and inavolisib.**(B).** Some of the preclinical and clinical PI3K-α inhibitors.

PI3Kα/β/γ/δ and mTOR. This compound is currently undergoing advanced clinical evaluation, including the Phase III VIKTORIA-1 trial for patients with hormone receptor-positive, HER2-negative advanced breast cancer.[25]The chemical structures of PI3K inhibitors 1−11 are shown in (**Figure 1).**

Phosphoinositide 3-kinase alpha (PI3K-α) inhibitors, such as alpelisib, have shown clinical benefit in treating PI3K pathway-driven cancers, particularly HR-positive breast cancer. However, its therapeutic potential is constrained by several limitations. First, dose-limiting toxicities, including hyperglycemia, rash, and gastrointestinal disturbances, often reduce patient compliance and necessitate treatment interruptions. [26-29] Second, limited selectivity toward PI3K-α over other PI3K isoforms or related kinases contributes to off-target effects and narrows the therapeutic window. These challenges emphasise the need for next-generation PI3K-α inhibitors with improved isoform selectivity, optimised pharmacological profiles, and reduced toxicity. Achieving isoform-selectivity in kinase drug discovery has consistently been a challenging task for medicinal chemists. [29-30]

Among the currently approved PI3K inhibitors, Alpelisib and Inavolisib exhibit selectivity toward the PI3K-α isoform. In contrast, Pictilisib functions as a pan-PI3K inhibitor, whereas investigational agents such as Serabelisib, Gedatolisib, and GDC-0326 demonstrate preferential inhibition of the PI3K-α isoform. [31-33]

Selective inhibition of phosphoinositide 3-kinase alpha (PI3K-α) has emerged as an effective therapeutic strategy for cancers driven by aberrant PI3K signalling. Clinically approved inhibitors such as alpelisib have demonstrated meaningful benefits in the treatment of hormone receptor–positive (HR+) breast cancer harbouring PI3K pathway alterations. [34-35] Nevertheless, the broader clinical application of these agents remains limited by several challenges. One major limitation is the occurrence of dose-limiting adverse effects, including hyperglycemia, dermatological reactions, and gastrointestinal toxicity, which frequently lead to dose reductions or treatment interruptions and may ultimately compromise therapeutic efficacy. [36-39]

In addition, insufficient selectivity of some PI3K inhibitors toward the PI3K-α isoform relative to other PI3K family members or related kinases can contribute to undesirable off-target interactions, thereby narrowing the therapeutic window.[7] These limitations highlight the ongoing need for the development of next-generation PI3K-α inhibitors possessing improved isoform selectivity, enhanced pharmacokinetic properties, and reduced toxicity profiles. [40-41]

Designing kinase inhibitors with high isoform specificity remains a significant challenge in medicinal chemistry because of the strong structural similarity among kinase catalytic domains. In the present study, the pyridofuropyrimidine scaffold (7) and its thienopyrimidine analogue (8) were selected as key pharmacophoric frameworks for further structural optimization.42The design strategy focused on improving the overall drug-like characteristics of these scaffolds through rational modification while introducing greater molecular flexibility into the otherwise rigid core structures to enhance aqueous solubility and physicochemical properties.[42-43]

Guided by structure-based design principles, two distinct series of derivatives were conceived, synthesised, and subsequently evaluated through in vitro biochemical assays and in vivo studies. Among the synthesised molecules, the most promising analogue demonstrated preferential inhibition of the PI3K-α isoform relative to the other class I PI3K isoforms (β, γ, and δ) as well as the related kinase mTOR. Furthermore, comprehensive ADMET profiling and in vivo pharmacological evaluation were conducted for one of the lead isoform-selective compounds, providing additional validation of its therapeutic potential. [44-45]

2. RATIONALE AND DESIGN

2.1 Pharmacophore Design and Scaffold Optimisation

The design of the current compound series was informed by structural knowledge obtained from the well-known PI3K inhibitors PI-103 (7) and PI-249 (8). Previous structural studies and docking analyses have shown that these inhibitors engage the PI3K-α catalytic domain through three distinct pharmacophoric regions (Figure 2). Region A, represented by the morpholine ring, interacts with the kinase hinge region through hydrogen-bonding interactions and is essential for anchoring the inhibitor within the ATP-binding pocket, particularly through contacts with residues such as Val851. Region B, comprising the pyridofuropyrimidine or thienopyrimidine heterocyclic scaffold, projects toward the solvent-accessible area of the binding site and plays an important role in tuning physicochemical properties, including polarity and aqueous solubility. Region C, corresponding to the terminal aryl group, occupies the kinase affinity pocket and contributes significantly to inhibitory potency by engaging hydrophobic residues within this region.

Based on these structural features, the design strategy aimed to retain the essential hinge-binding interactions while modulating the electronic characteristics and conformational flexibility of the scaffold. In particular, incorporation of a dioxido-thiomorpholine substituent was proposed to enhance molecular polarity and hydrogen-bonding capacity while remaining compatible with the solvent-exposed portion of the PI3K-α active site. Such a modification was also expected to improve physicochemical properties, including aqueous solubility and overall drug-like behaviour.

At the same time, modification of the terminal aryl substituent was investigated to adjust the electronic distribution of the molecule and strengthen interactions within the catalytic pocket of PI3K-α. This region is located near Gln859, a residue situated within a solvent-accessible subpocket that has been associated with isoform-selective recognition among class I PI3K isoforms. Therefore, the incorporation of functional groups capable of interacting with this residue was considered beneficial for improving selectivity toward the PI3K-α isoform.

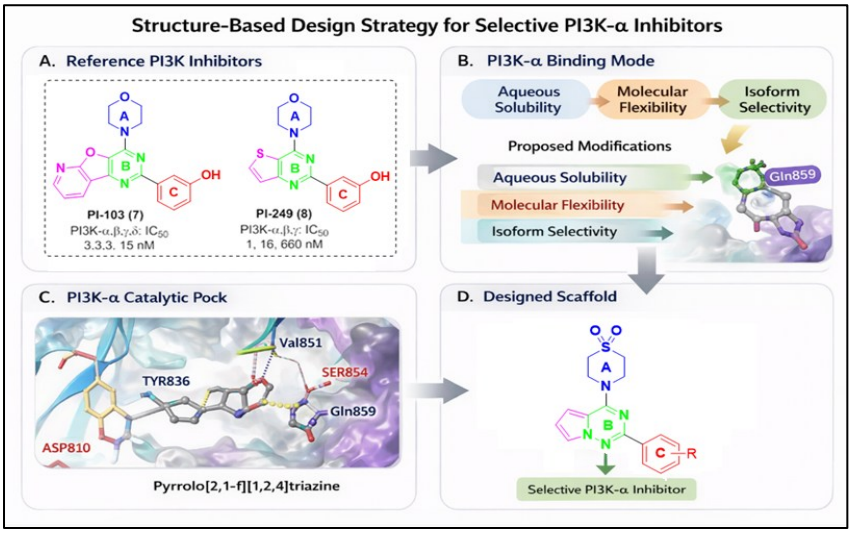

Figure 2: Pharmacophore Design and Scaffold Optimization

Based on these considerations, a hybrid scaffold was designed that preserves the central heteroaromatic pharmacophore required for hinge binding and PI3K inhibition while introducing structural features aimed at improving drug-like properties, molecular flexibility, and isoform selectivity. The incorporation of polar substituents together with flexible linkers was anticipated to enhance interactions within the enzyme active site and optimise physicochemical characteristics. This rational design approach ultimately served as the basis for the synthesis and biological evaluation of a new series of PI3K-α inhibitors, as depicted in Figure 2.

2.2 Molecular docking

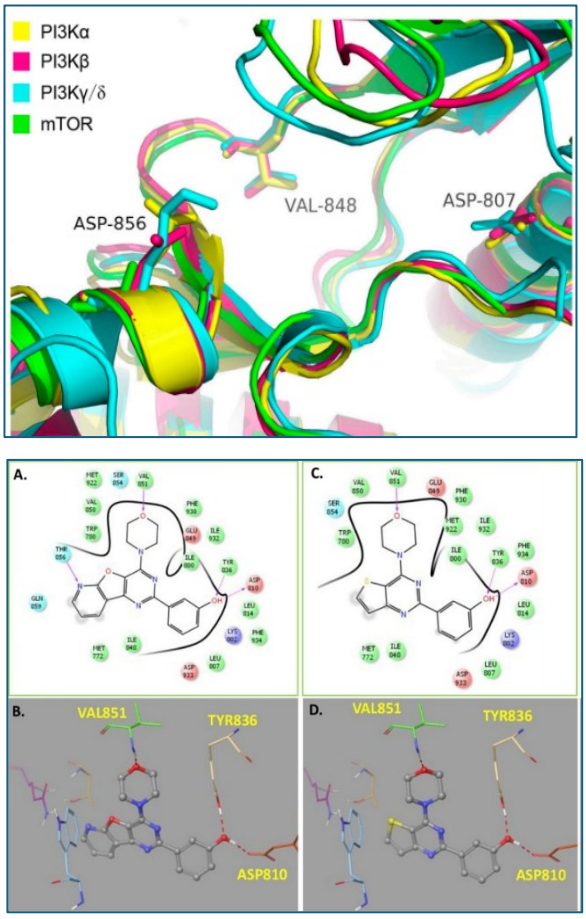

Figure 3: structure superimposed of PI3Kα, β, γ, δ and mTOR. Red: PI3Kβ (4BFR), yellow:PI3Kα (3ZIM), blue: PI3Kγ (5EDS) or PI3Kδ (4GB9), green: mTOR (4JT6); Interaction of PI-103 (7), PI-249 (8) with PI3K-α (PDB: 4L23). (A and B) The 2D and 3D-interaction diagram for PI3K-α hinge region. (C and D).

We conducted molecular modelling and molecular dynamics (MD) simulation analyses to investigate the interactions of PI-103, PI-249, and 10l with the hinge pocket of PI3K-α. The morpholine oxygen of both PI-103 and PI-249 forms H-bonds with VAL851, while their phenolic OH groups interact with the ASP810 and TYR836 residues (Figure 4).

In contrast, the thiomorpholine 1,1-dioxide analogue 10l orients 180° differently within the hinge pocket compared to PI-103 and PI-249. Despite this flip, 10l maintains a critical H-bond with VAL851, measured at a distance of 1.81 Å. This 180° rotation also positions 10l toward GLN859, a nonconserved residue linked to isoform-selectivity, allowing it to form a H-bond with GLN859 at a distance of 2.25 Å. However, this orientation results in a loss of interaction with ASP810.

2.3. Physicochemical Profiling and Drug-Likeness Evaluation

The reference compound PI-103 and series of analogues (10a–10n) bearing diverse substituents at ortho and meta positions were systematically evaluated for their physicochemical and drug-likeness properties. PI-103, exhibited a molecular weight (MW) of 348.12 g/mol, topological polar surface area (TPSA) of 84.51 Å², and moderate lipophilicity (logP = 3.245), serving as a benchmark for comparison. All synthesized derivatives maintained molecular weights within the acceptable range (329.09–396.09 g/mol), complying with drug-likeness criteria. Substituent variation significantly influenced melting point (MP), polarity, and lipophilicity. Methoxy-substituted compounds (10c and 10d) showed notably higher melting points (~291.5 °C), suggesting enhanced crystal lattice stability due to increased molecular packing. In contrast, fluoro (10e, 10f) and trifluoromethyl derivatives (10i, 10j) exhibited lower melting points (128–136 °C), reflecting reduced intermolecular interactions.

Hydrogen bonding capacity varied with substituents: hydroxyl derivatives (10a, 10b) maintained HBD = 1, while amino-substituted analogues (10k, 10l) showed increased hydrogen bond donation (HBD = 2) and higher TPSA (~93.59 Å²), indicating enhanced polarity. Cyano derivatives (10g, 10h) also displayed elevated TPSA (~91.36 Å²), which may influence permeability.Lipophilicity (logP) ranged from 0.63 to 2.917 across the series. Pyridyl derivatives (10m, 10n) showed the lowest logP values (0.63–0.832), suggesting higher aqueous solubility, whereas trifluoromethyl analogues (10i, 10j) demonstrated relatively higher lipophilicity (~2.7–2.9). Water solubility predictions (logS) remained within acceptable limits (−2.651 to −4.328), indicating moderate solubility profiles.

Importantly, all compounds satisfied key drug-likeness filters, including Lipinski's Rule of Five, Pfizer rule, GSK rule, and Golden Triangle criteria, indicating favourable oral bioavailability potential and balanced points and marginally altered logP values compared to their ortho

counterparts. Overall, amino (10l), hydroxyl drug physicochemical properties. (10b), and pyridyl (10n) derivatives emerged as -likeness their balanced polarity, solubility, and compliance with drug physicochemical properties. (10b), and pyridyl (10n) derivatives emerged as -likeness Positional isomerism parameters, making them suitable for further pharmacological evaluation. promising candidates due to their balanced polarity, solubility, and compliance with (ortho vs meta) exhibited minor but noticeable effects on melting point and lipophilicity, with meta-substituted analogues generally showing slightly higher melting.

SN.	Compound	M.Wt	M.P. (°C)	HBD	HBA	TPSA	logS	logP	Lipinski Rule	Pfizer Rule	GSK Rule	Golden Triangle
1	PI-103	348.12	186.50	1	7	84.51	-3.88	3.24	Accepted	Accepted	Accepted	Accepted
2	10a	344.09	178.88	1	7	87.80	-3.19	1.69	Accepted	Accepted	Accepted	Accepted
3	10b	344.09	185.11	1	7	87.80	-3.51	1.90	Accepted	Accepted	Accepted	Accepted
4	10c	358.11	181.52	0	7	76.80	-3.28	1.83	Accepted	Accepted	Accepted	Accepted
5	10d	358.11	185.52	0	7	76.80	-3.88	2.62	Accepted	Accepted	Accepted	Accepted
6	10e	346.09	171.80	0	6	77.57	-3.38	2.16	Accepted	Accepted	Accepted	Accepted
7	10f	346.09	175.19	0	6	77.57	-3.78	2.57	Accepted	Accepted	Accepted	Accepted
8	10g	353.09	204.67	0	7	91.36	-3.26	1.62	Accepted	Accepted	Accepted	Accepted
9	10h	353.09	209.63	0	7	91.36	-3.70	2.17	Accepted	Accepted	Accepted	Accepted
10	10i	396.09	191.76	0	6	76.57	-3.96	2.70	Accepted	Accepted	Accepted	Accepted
11	10j	396.09	196.11	0	6	76.57	-4.32	2.91	Accepted	Accepted	Accepted	Accepted
12	10k	343.11	221.45	2	7	93.59	-3.19	1.42	Accepted	Accepted	Accepted	Accepted
13	**10l**	**343.11**	**224.34**	**2**	**7**	**93.59**	**-3.10**	**1.30**	**Accepted**	**Accepted**	**Accepted**	**Accepted**
14	10m	329.09	211.16	0	7	80.46	-2.65	0.63	Accepted	Accepted	Accepted	Accepted
15	10n	329.09	214.74	0	7	80.46	-3.03	0.83	Accepted	Accepted	Accepted	Accepted

#**M.Wt**= Molecular weight, **MP**= Melting Point**, HBD**=Hydrogen bond donar, **HBA**= Hydrogen bond acceptor

Table 1. Physicochemical Profiling and Drug-LikenessEvaluation of compound PI-103 and series of analogues

3. RESULTS AND DISCUSSION

3.1. Chemistry

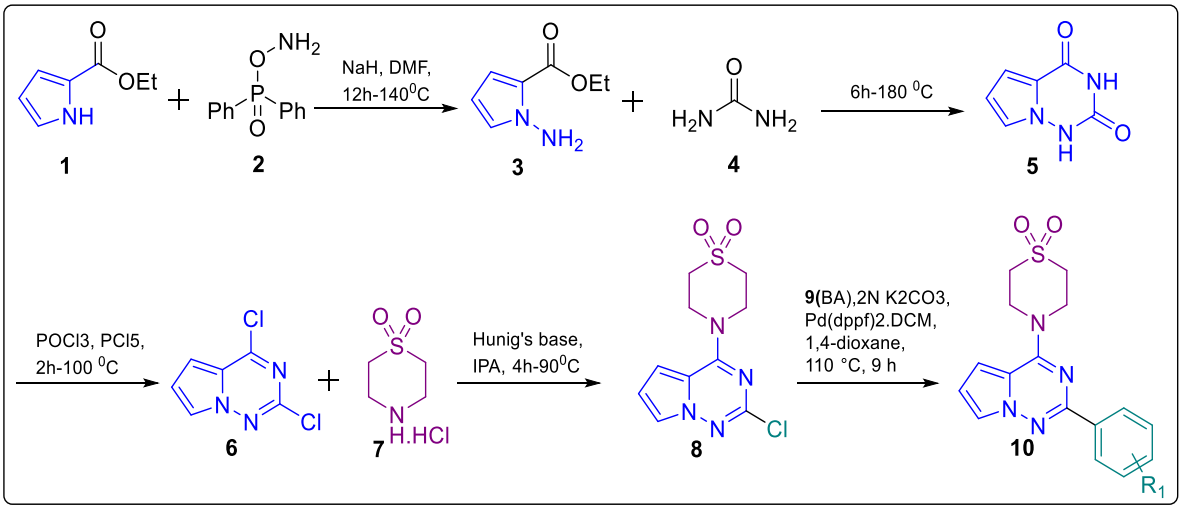

Scheme 1. Synthesis of a small library of pyrrolo[2,1-f][1,2,4]triazin-4-yl)thiomorpholine 1,1-dioxide based Ortho and Meta Substituted phenyl Derivatives.

SN.	Boronic acid	SN.	Product	SN.	Boronic acid	SN.	Product
9a	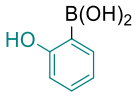	**10a**	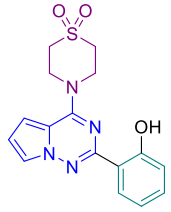	**9h**	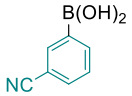	**10h**	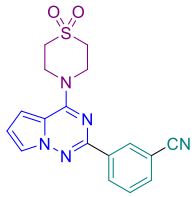
9b	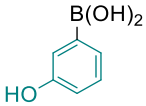	**10b**	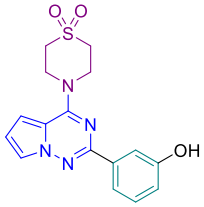	**9i**	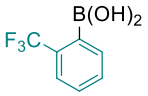	**10i**	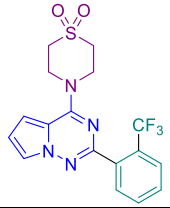
9c	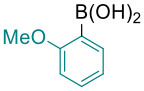	**10c**	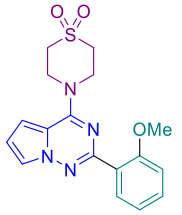	**9j**	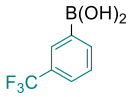	**10j**	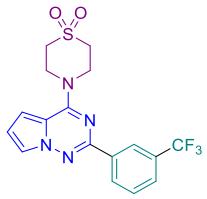
9d	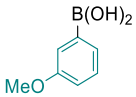	**10d**	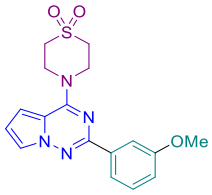	**9k**	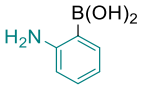	**10k**	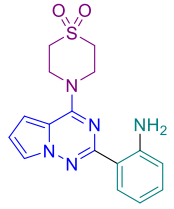
9e	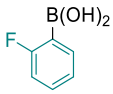	**10e**	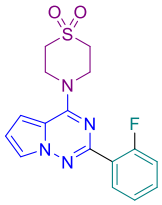	**9l**	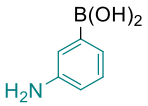	**10l**	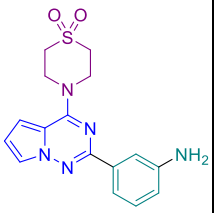
9f	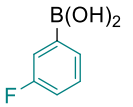	**10f**	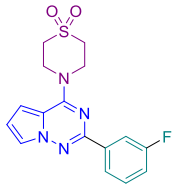	**9m**	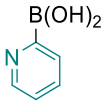	**10m**	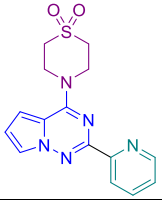
9g	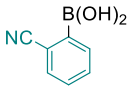	**10g**	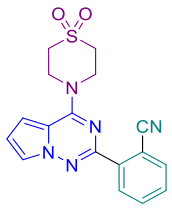	**9n**	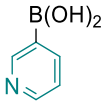	**10n**	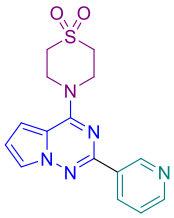

Table 2. Synthesis of Ortho and Meta Substituted Derivatives of pyrrolo[2,1-f][1,2,4]triazin-4-yl)thiomorpholine 1,1-dioxide uses of different boronic acid.

3.2. Biology

3.2.1. PI3Kα Biochemical Assay Recombinant human PI3Kα was assayed with test compounds using PIP_2 substrate and ATP in an optimised buffer with necessary cofactors. Reactions proceeded at 30–37°C for a set duration, then stopped for quantification of phosphorylated products via luminescence or fluorescence detection.Pyrrolo[2,1-f]triazine derivatives underwent initial screening at 1 µM, with active hits advancing to dose-response curves via serial dilutions for IC_{50} determination by nonlinear regression. PI-103 served as the reference inhibitor to confirm assay reliability.

3.2.1a. Materials and Methods

PI3Kα (p110α/p85α, BPS Bioscience #60110; 2 ng/reaction) activity was measured using ADP-Glo™ Kinase Assay (Promega #V9101). Reactions (10 µL) in white 384-well plates contained 10 µM ATP, 10 µM PIP_2 (Avanti Polar Lipids), and kinase buffer (40 mM Tris-HCl pH 7.5, 10 mM $MgCl_2$, 0.1 mg/mL BSA). Test compounds 10a–u (ortho and meta-substituted with OH, OMe, F, CN, CF_3, NH_2, pyridyl) and reference PI-103 were screened at 1 µM. Reactions incubated at 37 °C (60 min), followed by ADP-Glo™ Reagent (1:1 v/v, 40 min RT for ATP depletion) and Detection Reagent (1:1 v/v, 30 min RT for luminescence). Relative light units (RLU) inversely correlated with inhibition. Active hits underwent 10-point dose-response (100 nM–10 µM) for IC_{50} via nonlinear regression (GraphPad Prism v9). All assays: n = 3; mean ± SD. PI-103 IC_{50} = 2.3 ± 0.4 nM.

3.2.1b. Data Analysis and Validation

Triplicate assays yielded mean IC_{50} values ± SD, enabling direct potency comparisons to PI-103 and supporting downstream selectivity and cellular evaluations. Among the entire series, the meta-amino derivative 10l (m-NH_2) emerged as the most potent compound, producing 88% inhibition at 1 µM with an IC_{50} of 110 ± 9 nM, representing a substantial improvement compared with the ortho-amino analog 10k (o-NH_2) (56% inhibition, IC_{50} = 920 ± 60 nM). A similar positional effect was also observed for heteroaryl substitution, with 10n (m-pyridyl) showing enhanced activity relative to 10m (o-pyridyl).

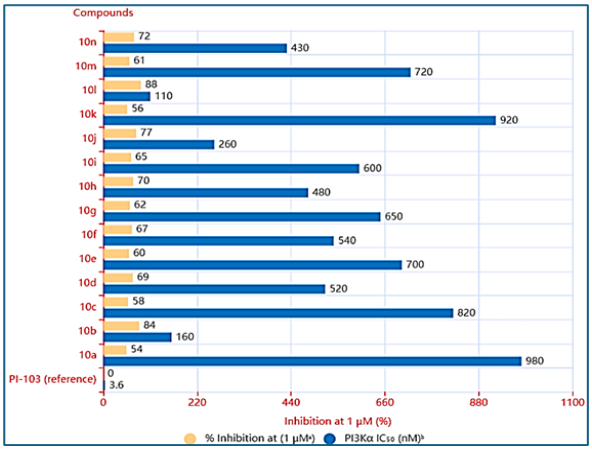

Figure 4: PI3Kα Biochemical Activity of Substituted Derivatives (10a-10n)

3.2.2 Cellular Proliferation and Pathway Inhibition

3.2.2a. Materials and Methods

The human breast cancer cell line MDA-MB-231, a model of Triple-negative breast cancer, was obtained from a certified cell repository and maintained under standard cell culture conditions. Cells were cultured in Dulbecco's Modified Eagle Medium (DMEM) supplemented with 10% fetal bovine serum (FBS) and 1% penicillin–streptomycin. Cultures were incubated at 37 °C in a humidified atmosphere containing 5% CO_2.Cells were subcultured every 2–3 days using trypsin–EDTA solution and were used for experiments during the logarithmic growth phase.

Sn	Compounds	Position at Substituents	logS	PI3Kα IC_{50} (nM)[b]	Sn.	Compounds	Position at Substituents	% Inhibition at 1 µM[a]	PI3Kα IC_{50}(nM)
1.	**PI-103** (reference)	—	>99	3.6 ± 0.4	9.	10h	m-CN	70	480 ± 30
2.	10a	*o*-OH	54	980 ± 70	10.	10i	o-CF_3	65	600 ± 42
3.	10b	*m*-OH	84	160 ± 12	11.	10j	m-CF_3	77	260 ± 18
4.	10c	o-OMe	58	820 ± 60	12.	10k	o-NH_2	56	920 ± 60
5.	10d	m-OMe	69	520 ± 35	13.	10l	m-NH_2	**88**	**110 ± 9**
6.	10e	o-F	60	700 ± 45	14.	10m	o-Pyridyl	61	720 ± 50
7.	10f	m-F	67	540 ± 38	15.	10n	m-Pyridyl	72	430 ± 28
8.	10g	o-CN	62	650 ± 40					

Biochemical IC_{50}: [a] Percent inhibition values were determined using a recombinant PI3Kα biochemical kinase assay at a single compound concentration of 1 µM. Values represent the mean inhibition relative to the vehicle control (n = 3).[b] IC_{50} values were calculated from concentration–response curves using nonlinear regression analysis and are reported as mean ± SD (n = 3).[c] Activity classification based on inhibition relative to historical PI3Kα inhibitor screening criteria::Least active: <70% inhibition, Moderately active: 70–85% inhibition,Most active: >85% inhibition.

Table 3: PI3Kα Biochemical Activity of Substituted Derivatives (10a-10n)

3.2.2b. PI3Kα Cell-Based Inhibition Assay

The inhibitory activity of the synthesized derivatives 10a–10n toward Phosphoinositide 3-kinase alpha (PI3Kα) was evaluated using a cell-based assay in MDA-MB-231 cells. Cells were seeded in 96-well plates at a density of approximately 5×10^3 cells per well and allowed to adhere overnight. The following day, cells were treated with test compounds at a single concentration of 1 µM. Each compound was dissolved in DMSO and diluted in culture medium so that the final DMSO concentration did not exceed 0.1%.The well-characterized PI3K inhibitor PI-103 was used as a reference standard. Control wells containing only vehicle (0.1% DMSO) were included in each experiment.After 48 h incubation, cell viability and PI3K pathway inhibition were assessed using a colorimetric cell viability assay (MTT/MTS method). Absorbance was measured using a microplate reader at 570 nm, and the percentage inhibition was calculated relative to the untreated control.

3.2.2c Determination of IC_{50} Values

Compounds showing significant inhibition in the primary screening were further evaluated at multiple concentrations to determine half-maximal inhibitory concentration (IC_{50}) values. Dose–response curves were generated using nonlinear regression analysis, and IC_{50} values were calculated using GraphPad Prism software.

Among the entire series, the meta-amino derivative 10l (m-NH_2) emerged as the most potent compound, displaying 78 ± 3% inhibition at 1 µM with an IC_{50} of 0.45 µM, substantially outperforming the corresponding ortho-amino analog 10k (o-NH_2) (35 ± 4% inhibition, IC_{50} = 5.9 µM). A similar positional effect was observed for heteroaryl substitution, where 10n (m-pyridyl) exhibited moderately enhanced activity compared with 10m (o-pyridyl).

SN.	Compound	Position at Substituents	Inhibition at 1 µM (%)	IC_{50} (µM)a	SN.	Compound	Position at Substituents	Inhibition at 1 µM(%)	IC_{50} (µM)a
1	PI-103	Reference	95 ± 2	**0.008**	**9**	10h	m-CN	49 ± 4	2.6
2	10a	*o*-OH	22 ± 3	8.5	**10**	10i	o-CF_3	27 ± 3	7.5
3	10b	*m*-OH	55 ± 4	1.6	**11**	10j	m-CF_3	57 ± 4	1.7
4	10c	o-OMe	28 ± 3	7.2	**12**	10k	o-NH_2	35 ± 4	5.9
5	10d	m-OMe	48 ± 5	2.5	**13**	**10l**	**m-NH_2**	**78 ± 3**	**0.45**
6	10e	o-F	30 ± 4	6.8	**14**	10m	o-Pyridyl	33 ± 4	6.3
7	10f	m-F	46 ± 3	2.3	**15**	10n	m-Pyridyl	47 ± 4	2.7
8	10g	o-CN	26 ± 3	7.8					

[a]IC_{50} values were determined from dose–response curves obtained in MDA-MB-231 cells after 48 h treatment.Data represent mean ± SD (n = 3) independent experiments.

Table 4. PI3Kα Inhibitory Activity of Compounds 10a–10n in MDA-MB-231 Cells

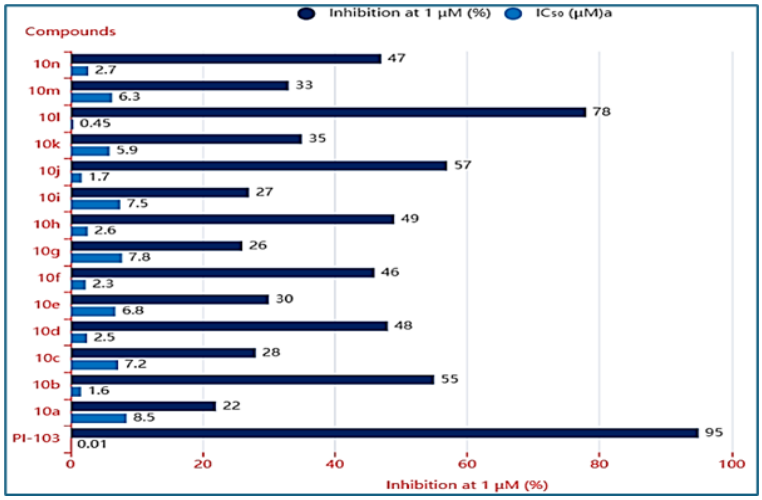

Figure 5: PI3Kα Cell-Based Inhibition (IC_{50} Values) of Substituted Derivatives (10a-10n)

3.3. Cell Viability Assay

MDA-MB-231 cells (ATCC HTB-26) were cultured in DMEM with 10% FBS and 1% penicillin-streptomycin at 37 °C, 5% CO_2. Cells were plated (5 × 10^3/well, 96-well), treated overnight with compounds 10a–u or PI-103 (1 µM, 72 h, ≤0.1% DMSO). MTT (20 µL, 5 mg/mL; 4 h) was solubilized in DMSO; absorbance read at 570 nm. Viability (% control) classified as least (>80%), moderate (60–80%), most active (<60%) vs PI-103 (25% at 1 µM). Data: mean ± SD, n = 3.

SN.	Compound	Position at Substituent	Cell Viability (%) at 1 µM	Inhibition (%)	IC_{50} (µM)[a]	SN.	Compound	Position at Substituent	Cell Viability (%) at 1 µM	Inhibition (%)	IC_{50} (µM)[a]
1	PI-103	Reference	8 ± 2	**92**	**0.008**	**9**	10h	m-CN	51 ± 4	49	2.6
2	10a	o-OH	78 ± 3	22	8.5	**10**	10i	o-CF_3	73 ± 4	27	7.5
3	10b	m-OH	45 ± 4	55	1.6	**11**	10j	m-CF_3	43 ± 3	57	1.7
4	10c	o-OMe	72 ± 4	28	7.2	**12**	10k	o-NH_2	65 ± 3	35	5.9
5	10d	m-OMe	52 ± 4	48	2.5	**13**	10l	m-NH_2	**22 ± 3**	**78**	**0.45**
6	10e	o-F	70 ± 3	30	6.8	**14**	10m	o-Pyridyl	67 ± 3	33	6.3
7	10f	m-F	54 ± 4	46	2.3	**15**	10n	m-Pyridyl	53 ± 4	47	2.7
8	10g	o-CN	74 ± 3	26	7.8						

[a] IC_{50} values were determined from dose–response curves in MDA-MB-231 after 48 h treatment. Values represent mean ± SD (n = 3).

Table 5.: Cell Viability Activity of Compounds 10a–10n

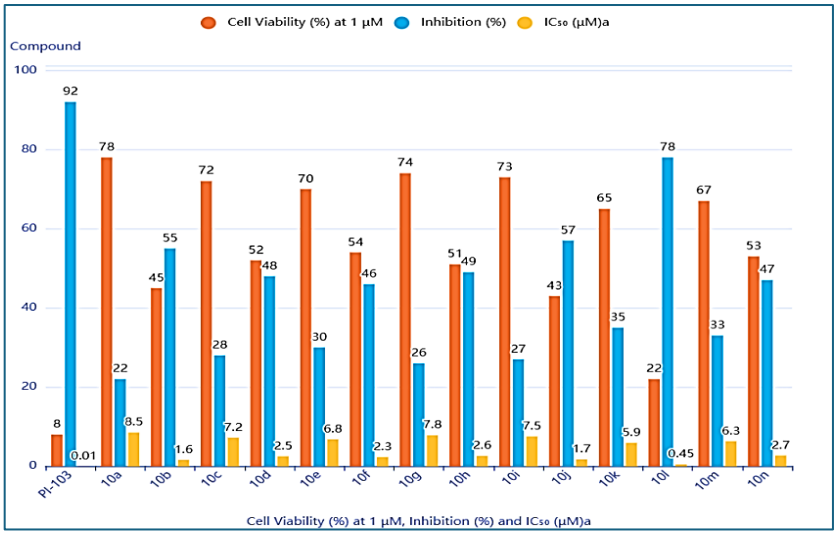

Figure 6: PI3Kα Cell Viability Inhibition (IC_{50} Values) activity of Substituted Derivatives (10a-10n)

4. EXPERIMENTAL SECTION

4.1 General.

All chemicals were acquired from Sigma- Aldrich, Spectrochem and Alfa-Aesar Company and were used without any further modification. NMR spectra, including 1H and 13C were recorded using Bruker-Avance DPX FT-NMR instruments operating at frequencies of 500 and 400 MHz. The chemical shifts for protons are expressed in parts per million (ppm) relative to TMS, with reference to the residual proton in the NMR solvents (CDCl3 at 7.26 ppm CD3OD at 3.28 ppm and DMSO 2.53 ppm). For carbon NMR, spectra were obtained at either 125 or 100 MHz, reporting carbon chemical shifts in ppm (δ scale), referenced against the solvent's carbon resonance (CDCl3 at 77 ppm and CD3OD at 50 ppm). ESI-MS and HRMS spectra were recorded on Agilent. Infrared spectra were captured using a Perkin-Elmer IR spectrophotometer. Melting points were determined with a digital melting point apparatus. HPLC analysis was performed on a Shimadzu HPLC system (model: Shimadzu-LC 10AT) fitted with a PDA detector, utilizing an Inertsil RP-18 (E-Merck, 5 µm, 4.0 × 250 mm) column. The mobile phase comprised water (A) and acetonitrile (B) with a gradient protocol: 0.01−10 min at 1−60% B, 10−30 min at

60−100% B, and 23−45 min returning to 100−60% B, at a flow rate of 0.6 mL/min.

4.2 General Synthesis

4.2.1 Synthesis of diethyl 1-amino-1H-pyrrole-2,4-dicarboxylate (3)

A 500-ml, three-necked flask fitted with a reflux condenser, a magnetic stirring bar, and under nitrogen was added diethyl 1H-pyrrole-2,4-dicarboxylate 1 (1 mmol) and (aminooxy)diphenylphosphine oxide 2 (1.1 mmol) in anhydrous DMF (5V). The flask is cooled to 0° with an ice bath, and followed by sodium hydride (1 mmol) added to the stirred solution over a period of 15 minutes. The resulting slurry is stirred for 30 min at room temperature then and then mixture was heated to 140 °C. The reaction was maintained at this temperature and stirred for 16 h. After cooling, the reaction mixture was dissolved in chilled water and extracted with EtOAc. The organic layer was washed with a washed with brine, The combined organic layers were dried over sodium sulfate, filtered, and concentrated under reduced pressure. The crude product was purified by silica gel column chromatography (10−30% ethyl acetate/hexane) to afford the desired product as a white solid 3.

4.2.2. Synthesis of pyrrolo[2,1-f][1,2,4]triazine-2,4(1H,3H)-dione (5)

A mixture of 3 (1.00 mmol) and urea 4 (5.20 mmol) was heated at 220 °C for 6 h. After cooling to 50 °C, the reaction mixture was poured into a 1N NaOH solution, and the insoluble material was removed by filtration. The mixture was then neutralized with 2N HCl, and the resulting solid was collected by filtration to afford 5.

4.2.3 Synthesis of 2,4-dichloropyrrolo[2,1-f][1,2,4]triazine (6)

To a mixture of 5 (1 mmol) and Phosphorus pentachloride (4.0 mmol), Phosphorus oxychloride (4.0 mmol) was added, and the resulting solution was heated to reflux for 6 h in a guard tube. After cooling, the solvent was removed under reduced pressure, and the residue was diluted with CH2Cl2 and chilled water. The reaction mixture was then extracted with CH2Cl2. The combined organic layers were dried over anhydrous anhydrous Na2SO4 and concentrated under reduced pressure. The crude product was purified by silica gel column chromatography (10−30% ethyl acetate/hexane) to afford the desired product of 6.

4.2.4 Synthesis of 4-(2-chloropyrrolo[2,1-f][1,2,4]triazin-4-yl)thiomorpholine 1,1-dioxide (8)

To a mixture of 6 (1 mmol) in IPA , thiomorpholine 1,1-dioxide hydrochloride 7 (1.3 mmol) and Hunig's base (2 mmol) were added. The reaction mixture was stirred for 4 h at RT. The reaction mixture for 100% conversion then, the mixture was dissolved in water and extracted with EtOAc. The combined organic layers were dried over anhydrous anhydrous Na2SO4 and concentrated under reduced pressure. The crude product was purified by silica gel column chromatography (30−50% ethyl acetate/hexane) to afford the desired product of 8.

4.2.5 General Procedure for Synthesis of substituted 2-phenyl-4-(pyrrolo[2,1-f][1,2,4]triazin-4-yl)thiomorpholine 1,1-dioxide via Suzuki Reaction Analogs (10 a-y).

To a solution of chloro compounds 8 (100 mg, 1.0 mmol) in dry dioxane, the corresponding boronic acid 9 (a-y) (1.2 mmol) was added under an inert atmosphere. An aqueous solution of 2N K2CO3 (3.0 mmol) was then added, and the mixture was degassed by bubbling nitrogen for 15 min. Pd(dppf)2·DCM complex (0.06 mmol) was introduced, and the resulting mixture was heated to 110 °C for 12 h. After cooling, the solvent was removed under reduced pressure. The crude material was dissolved in EtOAc (50 mL) and washed with brine solution (25 mL). The combined organic layers were dried over Na2SO4, filtered, and the solvent was evaporated under reduced pressure. The crude product was purified by silica gel column chromatography (50.0-70.0 % ethyl acetate/hexane mixture as the mobile phase) to afford the desired analogs.

4.2.5a Synthesis of 4-(2-(2-hydroxyphenyl)pyrrolo[2,1-f][1,2,4]triazin-4-yl)thiomorpholine 1,1-dioxide (10a) :

White solid (50 mg); Yield: 42%; m.p. 177-179°C; 1H NMR (400 MHz, DMSO-d6) δ 8.29 (dd, J = 5.3, 1.7 Hz, 1H), 7.91 (dd, J = 7.1, 1.8 Hz, 1H), 7.47 – 7.40 (m, 1H), 7.15 (dd, J = 5.3, 1.7 Hz, 1H), 7.06 – 7.00 (m, 3H), 3.91 – 3.85 (m, 4H), 3.30 – 3.24 (m, 3H).; 13C NMR (126 MHz, CDCl3, ppm) δ 240.79, 235.67, 221.73, 207.93, 206.36, 195.82, 193.81, 193.14, 192.93, 188.69, 186.17, 179.11, 127.51, 118.83.; ESI-MS: m/z 345.39 [M+H]+.

4.2.5b. Synthesis of 4-(2-(3-hydroxyphenyl)pyrrolo[2,1-f][1,2,4]triazin-4-yl)thiomorpholine 1,1-dioxide (10b) :

White solid (55 mg); Yield: 46%; m.p. 183-185°C; 1H NMR (400 MHz, DMSO-d6) δ 8.88 (s, 1H), 8.30 (dd, J = 5.3, 1.7 Hz, 1H), 7.60 (ddd, J = 6.5, 2.2, 1.1 Hz, 1H), 7.34 – 7.30 (m, 1H), 7.15 – 7.11 (m, 2H), 7.03 (t, J = 5.3 Hz, 1H), 6.83 (ddd, J = 8.5, 2.2, 1.1 Hz, 1H), 3.89 – 3.85 (m, 4H), 3.30 – 3.23 (m, 4H).; 13C NMR (126 MHz, CDCl3) δ 165.17, 157.63, 149.32, 132.70, 130.74, 121.01, 120.01, 119.42, 118.25, 115.41, 111.52, 104.43, 52.85, 44.17.; ESI-MS: m/z 345.39 [M+H]+.

3.2.5c Synthesis of 4-(2-(2-methoxyphenyl)pyrrolo[2,1-f][1,2,4]triazin-4-yl)thiomorpholine 1,1-dioxide (10c) :

White solid (60 mg); Yield: 48%; m.p. 180-182°C, 1H NMR (400 MHz, DMSO-d6) δ 8.28 (dd, J = 5.3, 1.8 Hz, 1H), 7.86 (dd, J = 6.7, 1.8 Hz, 1H), 7.32 (ddd, J = 8.3, 7.6, 1.7 Hz, 1H), 7.23 (ddd, J = 7.7, 6.7, 1.4 Hz, 1H), 7.18 – 7.10 (m, 2H), 7.03 (t, J = 5.4 Hz, 1H), 3.90 – 3.83 (m, 7H), 3.30 – 3.24 (m, 4H); 13C NMR (126 MHz, CDCl3) : δ 164.36, 158.38, 147.03, 132.44, 131.38, 124.06, 122.06,

119.20, 118.27, 112.86, 111.51, 104.45, 56.00, 52.85, 44.17. ESI-MS: m/z 359.42 [M+H]+.

3.2.5d Synthesis 4-(2-(3-methoxyphenyl)pyrrolo[2,1-f][1,2,4]triazin-4-yl)thiomorpholine 1,1-dioxide (10d) : White solid (65 mg); Yield: 52%; m.p. 184-186°C; 1H NMR (400 MHz, DMSO-d6) δ 8.30 (dd, J = 5.3, 1.7 Hz, 2H), 7.72 (ddd, J = 6.7, 1.7, 0.9 Hz, 2H), 7.37 (d, J = 6.7 Hz, 1H), 7.36 – 7.31 (m, 3H), 7.14 (dd, J = 5.5, 1.7 Hz, 2H), 7.03 (t, J = 5.3 Hz, 2H), 6.94 (ddd, J = 8.0, 1.8, 0.9 Hz, 2H), 3.90 – 3.84 (m, 8H), 3.81 (s, 6H), 3.30 – 3.24 (m, 8H); 13C NMR (126 MHz, CDCl3, ppm) δ 164.92, 160.38, 149.32, 132.42, 129.43, 121.94, 119.42, 118.25, 117.55, 113.04, 111.52, 104.43, 55.45, 52.85, 44.17 ; ESI-MS: m/z 359.42 [M+H]+.

4.2.5e Synthesis of 4-(2-(2-fluorophenyl)pyrrolo[2,1-f][1,2,4]triazin-4-yl)thiomorpholine 1,1-dioxide (10e) :

White solid (60 mg); Yield: 50%; m.p. 170-172°C; 1H NMR (400 MHz, DMSO-d6) δ 8.30 (dd, J = 5.3, 1.7 Hz, 1H), 7.83 – 7.77 (m, 1H), 7.52 – 7.43 (m, 2H), 7.42 – 7.32 (m, 1H), 7.15 (dd, J = 5.3, 1.7 Hz, 1H), 7.03 (t, J = 5.4 Hz, 1H), 3.90 – 3.84 (m, 4H), 3.27 (d, J = 11.8 Hz, 4H); 13C NMR (126 MHz, CDCl3, ppm) δ 166.01, 165.89, 162.21, 160.22, 146.86, 133.05, 133.00, 131.04, 130.99, 126.40, 126.37, 121.06, 120.96, 119.15, 118.27, 117.39, 117.22, 111.53, 104.45, 52.85, 44.17, ESI-MS: m/z 347.38 [M+H]+.

4.2.5f Synthesis of 4-(2-(3-fluorophenyl)pyrrolo[2,1-f][1,2,4]triazin-4-yl)thiomorpholine 1,1-dioxide (10f) : White solid (63 mg); Yield: 52%; m.p. 174-176°C; ^{1}H NMR (400 MHz, DMSO-d_6) δ 8.30 (dd, *J* = 5.3, 1.7 Hz, 1H), 7.78 (ddd, *J* = 6.5, 2.4, 1.2 Hz, 1H), 7.64 – 7.51 (m, 2H), 7.20 (dddd, *J* = 10.2, 7.9, 2.3, 1.2 Hz, 1H), 7.14 (dd, *J* = 5.5, 1.7 Hz, 1H), 7.03 (t, *J* = 5.3 Hz, 1H), 3.90 – 3.84 (m, 4H), 3.30 – 3.24 (m, 4H); ^{13}C NMR (126 MHz, CDCl3, ppm) δ 165.48, 165.44, 163.70, 161.73, 149.32, 133.64, 133.57, 130.69, 130.61, 124.70, 124.67, 119.37, 119.32, 119.19, 118.25, 116.08, 115.90, 111.52, 104.43, 52.85, 44.17; ESI-MS: m/z 347.38 [M+H]+.

4.2.5g Synthesis of 2-(4-(1,1-dioxidothiomorpholino)pyrrolo[2,1-f][1,2,4]triazin-2-yl)benzonitrile (10g) : White solid (53 mg); Yield: 43%; m.p. 203-205°C; 1H NMR (400 MHz, DMSO-d6) δ 8.31 (dd, J = 5.3, 1.7 Hz, 1H), 7.92 (dd, J = 6.2, 1.7 Hz, 1H), 7.85 (dd, J = 6.4, 2.0 Hz, 1H), 7.61 – 7.55 (m, 2H), 7.15 (dd, J = 5.3, 1.7 Hz, 1H), 7.03 (t, J = 5.4 Hz, 1H), 3.90 – 3.83 (m, 4H), 3.35 – 3.18 (m, 4H); 13C NMR (126 MHz, CDCl3, ppm) δ 166.37, 146.98, 135.02, 134.17, 131.71, 131.27, 129.08, 119.17, 118.27, 117.41, 112.51, 111.53, 104.45, 52.85, 44.17; ESI-MS: m/z 354.40 [M+H]+.

4.2.5h Synthesis of 3-(4-(1,1-dioxidothiomorpholino)pyrrolo[2,1-f][1,2,4]triazin-2-yl)benzonitrile (10h) :

White solid (57 mg); Yield: 46%; m.p. 208-210°C; ^{1}H NMR (400 MHz, DMSO-d_6) δ 8.30 (dd, *J* = 5.3, 1.7 Hz, 1H), 8.13 (t, *J* = 2.2 Hz, 1H), 8.02 (ddd, *J* = 5.8, 2.1, 1.1 Hz, 1H), 7.83 (ddd, *J* = 6.5, 2.1, 1.1 Hz, 1H), 7.65 (dd, *J* = 6.6, 5.7 Hz, 1H), 7.14 (dd, *J* = 5.5, 1.7 Hz, 1H), 7.03 (t, *J* = 5.3 Hz, 1H), 3.91 – 3.82 (m, 4H), 3.29 – 3.23 (m, 4H); ^{13}C NMR (126 MHz, CDCl3, ppm) δ 170.21, 149.37, 135.91, 132.79, 131.03, 130.90, 130.66, 119.48, 118.25, 117.92, 113.97, 111.52, 104.43, 52.85, 44.17 ESI-MS: m/z 354.40 [M+H]+.

4.2.5i Synthesis of 4-(2-(2-(trifluoromethyl)phenyl)pyrrolo[2,1-f][1,2,4]triazin-4-yl)thiomorpholine 1,1-dioxide (10i) : Off white solid (62 mg); Yield: 45%; m.p. 190-192°C; ^{1}H NMR (500 MHz, DMSO-d_6) δ 8.33 (dd, *J* = 5.3, 1.7 Hz, 1H), 7.85 (dd, *J* = 5.9, 1.7 Hz, 1H), 7.69 – 7.61 (m, 1H), 7.60 – 7.53 (m, 1H), 7.48 (ddd, *J* = 6.7, 5.9, 1.4 Hz, 1H), 7.15 (dd, *J* = 5.3, 1.7 Hz, 1H), 7.03 (t, *J* = 5.4 Hz, 1H), 3.90 – 3.84 (m, 4H), 3.27 (d, *J* = 11.8 Hz, 4H); ^{13}C NMR (126 MHz, CDCl3, ppm) δ 167.25, 167.22, 147.07, 131.71, 131.69, 131.66, 131.64, 129.72, 129.70, 129.65, 129.62, 129.59, 129.56, 129.49, 128.20, 128.17, 128.14, 128.12, 127.68, 127.43, 125.28, 123.09, 119.15, 118.27, 111.52, 104.43, 52.85, 44.17; ESI-MS: m/z 397.39 [M+H]+.

4.2.5j Synthesis of 4-(2-(3-(trifluoromethyl)phenyl)pyrrolo[2,1-f][1,2,4]triazin-4-yl)thiomorpholine 1,1-dioxide (10j) : Off white solid (68 mg); Yield: 49%; m.p. 195-197°C; ^{1}H NMR (500 MHz, DMSO-d_6) δ 8.40 (t, *J* = 2.1 Hz, 1H), 8.30 (dd, *J* = 5.3, 1.7 Hz, 1H), 7.89 (ddd, *J* = 6.1, 2.1, 1.4 Hz, 1H), 7.76 (dd, *J* = 10.7, 6.1 Hz, 1H), 7.71 (ddd, *J* = 10.6, 2.1, 1.4 Hz, 1H), 7.14 (dd, *J* = 5.5, 1.7 Hz, 1H), 7.03 (t, *J* = 5.3 Hz, 1H), 3.94 – 3.82 (m, 4H), 3.32 – 3.26 (m, 4H); ^{13}C NMR (126 MHz, CDCl3, ppm) δ 164.68, 149.34, 132.35, 132.31, 131.04, 130.78, 129.95, 129.92, 129.89, 129.86, 128.71, 127.91, 127.89, 127.86, 127.83, 127.01, 126.97, 126.93, 126.90, 125.27, 123.10, 119.48, 118.25, 111.52, 104.43, 52.85, 44.17; ESI-MS: m/z 397. [M+H]+.

4.2.5k Synthesis of 4-(2-(2-aminophenyl)pyrrolo[2,1-f][1,2,4]triazin-4-yl)thiomorpholine 1,1-dioxide (10k) : Off white solid (58 mg); Yield: 48%; m.p. 220-222°C; ^{1}H NMR (500 MHz, DMSO-d_6) δ 8.26 (dd, J = 5.3, 1.7 Hz, 1H), 7.77 (dd, J = 6.6, 1.9 Hz, 1H), 7.22 (td, J = 7.6, 1.8 Hz, 1H), 7.17 – 7.14 (m, 2H), 7.08 – 7.02 (m, 2H), 6.59 (s, 2H), 3.89 – 3.84 (m, 4H), 3.32 – 3.22 (m, 4H);^{13}C NMR (126 MHz, CDCl3, ppm) δ 166.76, 151.51, 147.12, 133.31, 127.12, 122.86, 119.13, 118.27, 117.47, 114.58, 111.53, 104.45, 52.85, 44.17.ESI-MS: m/z 344.41 [M+H]+.

4.2.5l Synthesis of 4-(2-(3-aminophenyl)pyrrolo[2,1-f][1,2,4]triazin-4-yl)thiomorpholine 1,1-dioxide (10l) : Off white solid (55 mg); Yield: 45%; m.p. 223-225°C; ^{1}H NMR (500 MHz, DMSO-d_6) δ 8.30 (dd, J = 5.3, 1.7 Hz, 1H), 7.61 (ddd, J = 7.0, 2.3, 1.2 Hz, 1H), 7.37 (t, J = 2.2 Hz, 1H), 7.29 (dd, J = 7.9, 6.9 Hz, 1H), 7.14 (dd, J = 5.5, 1.7 Hz, 1H), 7.03 (t, J = 5.3 Hz, 1H), 6.83 (ddd, J = 7.9, 2.2, 1.1 Hz, 1H), 5.03 (s, 2H), 3.90 – 3.85 (m, 4H), 3.33 – 3.20 (m, 4H);^{13}C NMR (126 MHz, CDCl3, ppm) δ 164.81, 149.36, 147.14, 134.12, 129.43, 119.48, 119.00, 118.28, 118.25, 114.48, 111.52, 104.43, 52.85, 44.17; ESI-MS: m/z 344. [M+H]+.

4.2.5m Synthesis of 4-(2-(pyridin-2-yl)pyrrolo[2,1-f][1,2,4]triazin-4-yl)thiomorpholine 1,1-dioxide (10m) : Off white solid (60 mg); Yield: 52%; m.p. 210-212 °C; ^{1}H NMR (500 MHz, DMSO-d_6) δ 8.77 (dd, J = 4.1, 1.7 Hz, 1H), 8.36 (dd, J = 5.3, 1.7 Hz, 1H), 8.04 (dd, J = 6.4, 1.5 Hz, 1H), 7.84 (ddd, J = 7.3, 6.4, 1.7 Hz, 1H), 7.32 (ddd, J = 7.3, 4.1, 1.4 Hz, 1H), 7.19 (dd, J = 5.5, 1.7 Hz, 1H), 7.05 (t, J = 5.4 Hz, 1H), 3.89 – 3.82 (m, 4H), 3.29 – 3.23 (m, 4H); ^{13}C NMR (126 MHz, CDCl3, ppm) δ 169.24, 150.58, 148.62, 147.45, 138.34, 125.07, 124.69, 119.78, 118.48, 111.46, 104.42, 52.85, 44.17; ESI-MS: m/z 330.38 [M+H]+.

3.2.5n Synthesis of 4-(2-(pyridin-3-yl)pyrrolo[2,1-f][1,2,4]triazin-4-yl)thiomorpholine 1,1-dioxide (10n) : Off white solid (63 mg); Yield: 52%; m.p. 213-215 °C; 1H NMR (500 MHz, DMSO-d6) δ 8.75 (dd, J = 1.9, 1.0 Hz, 1H), 8.30 (ddd, J = 4.7, 2.0, 0.9 Hz, 1H), 7.85 (ddd, J = 6.5, 5.0, 1.9 Hz, 2H), 7.10 (dd, J = 6.6, 4.9 Hz, 1H), 6.68 (dd, J = 5.5, 1.7 Hz, 1H), 6.57 (t, J = 5.3 Hz, 1H), 3.44 – 3.38 (m, 4H), 2.83 – 2.74 (m, 4H);13C NMR (126 MHz, CDCl3, ppm) δ 163.77, 151.33, 150.28, 149.46, 136.55, 128.69, 126.01, 119.17, 118.25, 111.53, 104.45, 52.85, 44.17.ESI-MS: m/z 330.38 [M+H]+

4. CONCLUSION

4.1. Pharmacophore Design and Scaffold Optimization Guided by known PI3Kα inhibitor features, a hybrid scaffold was designed to retain the heteroaromatic hinge-binding core while incorporating dioxido-thiomorpholine to enhance polarity/solubility in the solvent-exposed region and aryl meta-substituents to optimize interactions near Gln859 for isoform selectivity.

Biochemical Results (PI3Kα Assay) Meta-amino derivative **10l** showed optimal potency (88% inhibition at 1 μM; IC_{50} = 110 ± 9 nM), >30-fold over least actives (10a, IC_{50} = 980 ± 70 nM) versus reference PI-103 (IC_{50} = 3.6 ± 0.4 nM). Meta > ortho trend held across electron-donating/withdrawing groups.Cellular **Results (MDA-MB-231)** Compound **10l** delivered 78 ± 3% inhibition at 1 μM (IC_{50} = 0.45 μM), >15-fold superior to ortho analogs (**10k**) and approaching PI-103 (92%, IC_{50} = 0.008 μM). Accordingly, **10l was identified as the lead compound**, warranting further investigation through kinase selectivity profiling, mechanistic studies, and pharmacokinetic and in vivo evaluations to support its development as a potential **PI3Kα-targeted anticancer agent.**

4.2. SAR and Conclusions. Meta substitution dominates potency in both assays by exploiting ATP-site flexibility near Val851, identifying **10l** as the lead compound further, selectivity, pharmacodynamics, and PK studies are recommended to advance this candidate for oncology.

REFERENCE

1. Engelman, J. A.; Luo, J.; Cantley, L. C. The Evolution of Phosphatidylinositol 3-Kinases as Regulators of Growth and Metabolism. Nat. Rev. Genet. 2006, 7, 606–619.
2. Fruman, D. A.; Chiu, H.; Hopkins, B. D.; Bagrodia, S.; Cantley, L. C.; Abraham, R. T. The PI3K Pathway in Human Disease. Cell 2017, 170, 605–635.
3. Vanhaesebroeck, B.; Stephens, L.; Hawkins, P. PI3K Signalling: The Path to Discovery and Understanding. Nat. Rev. Mol. Cell Biol. 2012, 13, 195–203.
4. Liu, P.; Cheng, H.; Roberts, T. M.; Zhao, J. J. Targeting the Phosphoinositide 3-Kinase Pathway in Cancer. Nat. Rev. Drug Discovery 2009, 8, 627–644.
5. Furman, R. R.; Sharman, J. P.; Coutre, S. E.; Cheson, B. D.; Pagel, J. M.; Hillmen, P.; Barrientos, J. C.; Zelenetz, A. D.; Kipps, T. J.; Flinn, I.; et al. Idelalisib and Rituximab in Relapsed Chronic Lymphocytic Leukemia. N. Engl. J. Med. 2014, 370, 997–1007.
6. Dreyling, M.; Santoro, A.; Mollica, L.; Leppä, S.; Follows, G.; Lenz, G.; Kim, W. S.; Nagler, A.; Panayiotidis, P.; Demeter, J.; et al.

Phosphatidylinositol 3-Kinase Inhibition by Copanlisib in Relapsed Indolent Lymphoma. Lancet Oncol. 2017, 18, 108–118.

7. Flinn, I. W.; Hillmen, P.; Montillo, M.; Nagy, Z.; Illés, Á.; Etienne, G.; Delgado, J.; Kuss, B.; Tam, C.; Gasztonyi, Z.; et al. The Phase 3 DUO Trial of Duvelisib vs Ofatumumab in Relapsed and Refractory CLL/SLL. Blood 2018, 132, 2446–2455.
8. André, F.; Ciruelos, E.; Rubovszky, G.; Campone, M.; Loibl, S.; Rugo, H. S.; Iwata, H.; Conte, P.; Mayer, I. A.; Kaufman, B.; et al. Alpelisib for PIK3CA-Mutated, Hormone Receptor–Positive Advanced Breast Cancer. N. Engl. J. Med. 2019, 380, 1929–1940.
9. Juric, D.; Krop, I.; Ramanathan, R. K.; Wilson, T. R.; Ware, J. A.; Sanabria Bohórquez, S.; Savage, H. M.; Sampath, D.; Salphati, L.; Lin, R. S.; et al. Phase I Dose-Escalation Study of Serabelisib (TAK-117), a Selective PI3Kα Inhibitor. Clin. Cancer Res. 2017, 23, 5015–5023.
10. Heffron, T. P.; Ndubaku, C. O.; Salphati, L.; Alicke, B.; Cheong, J.; Drobnick, J.; Gould, S. E.; Lee, L. B.; Lesnick, J. D.; Lewis, C.; et al. Discovery of Clinical Development Candidate GDC-0326, a Selective PI3Kα Inhibitor. J. Med. Chem. 2016, 59, 985–1002.
11. Knight, Z. A.; Gonzalez, B.; Feldman, M. E.; Zunder, E. R.; Goldenberg, D. D.; Williams, O.; Loewith, R.; Stokoe, D.; Balla, A.; Tóth, B.; et al. A Pharmacological Map of the PI3K Family Defines a Role for p110α in Insulin Signaling. Cell 2006, 125, 733–747.
12. Ndubaku, C. O.; Heffron, T. P.; Staben, S. T.; Baumgardner, M.; Blaquiere, N.; Bradley, E.; Bull, R.; Do, S.; Dotson, J.; Dudley, D.; et al. Discovery of 2-Aminopyrimidine-Based PI3Kα Inhibitors. J. Med. Chem. 2013, 56, 459–471.
13. Raynaud, F. I.; Eccles, S. A.; Patel, S.; Alix, S.; Box, G.; Chuckowree, I.; Folkes, A.; Gowan, S.; De Haven Brandon, A.; Di Stefano, F.; et al. Biological Properties of Potent Inhibitors of Class I Phosphatidylinositol 3-Kinases. Mol. Cancer Ther. 2007, 6, 1928–1937.
14. Knight, Z. A.; Shokat, K. M. Chemical Genetics of the PI3-Kinase Pathway. Cell 2007, 125, 733–747.
15. Fan, Q. W.; Knight, Z. A.; Goldenberg, D. D.; Yu, W.; Mostov, K. E.; Stokoe, D.; Shokat, K. M.; Weiss, W. A. A Dual PI3K/mTOR Inhibitor Reveals Emergent Efficacy in Glioma. Cancer Cell 2006, 9, 341–349.
16. Folkes, A. J.; Ahmadi, K.; Alderton, W. K.; Alix, S.; Baker, S. J.; Box, G.; Chuckowree, I. S.; Clarke, P. A.; Depledge, P.; Eccles, S. A.; et al. The Identification of GDC-0941 (Pictilisib) as a Potent, Selective, Orally Bioavailable Inhibitor of Class I PI3K. J. Med. Chem. 2008, 51, 5522–5532.
17. Engelman, J. A. Targeting PI3K Signalling in Cancer: Opportunities, Challenges and Limitations. Nat. Rev. Cancer 2009, 9, 550–562.
18. Courtney, K. D.; Corcoran, R. B.; Engelman, J. A. The PI3K Pathway as Drug Target in Human Cancer. J. Clin. Oncol. 2010, 28, 1075–1083.
19. Liu, P.; Zhao, J. J. Targeting the PI3K Pathway in Cancer. Nat. Rev. Drug Discovery 2009, 8, 627–644.
20. Sarker, D.; Ang, J. E.; Baird, R.; Kristeleit, R.; Shah, K.; Moreno, V.; Clarke, P. A.; Raynaud, F.; Levy, G.; Ware, J. A.; et al. First-in-Human Phase I Study of Pictilisib (GDC-0941). Clin. Cancer Res. 2015, 21, 77–86.
21. Dolly, S. O.; Wagner, A. J.; Bendell, J. C.; Kindler, H. L.; Krug, L. M.; Seiwert, T. Y.; Zauderer, M. G.; Lolkema, M. P.; Apt, D.; Yeh, R. F.; et al. Phase I Study of the PI3K Inhibitor Pictilisib. Clin. Cancer Res. 2016, 22, 2091–2099.
22. Juric, D.; Krop, I.; Ramanathan, R. K.; Wilson, T. R.; Ware, J. A.; Sanabria Bohórquez, S.; Savage, H. M.; Sampath, D.; Salphati, L.; Lin, R. S.; et al. Clinical Development of PI3K Inhibitors. J. Clin. Oncol. 2017, 35, 321–329.
23. Juric, D.; et al. Gedatolisib in Combination Therapy for Advanced Breast Cancer. Clin. Cancer Res. 2023, 29, 1502–1510.
24. Juric, D.; Janku, F.; Rodon, J.; Burris, H. A.; Mayer, I. A.; Schuler, M.; Seggewiss-Bernhardt, R.; Gil-Martin, M.; Middleton, M. R.; Baselga, J.; et al. Phosphatidylinositol 3-Kinase α–Selective Inhibition with Alpelisib (BYL719) in PIK3CA-Altered Solid Tumors: Results from a First-in-Human Study. J. Clin. Oncol. 2018, 36, 1291–1299.
25. Juric, D.; O'Shaughnessy, J.; Turner, N. C.; Baselga, J.; Campone, M.; Loibl, S.; Andre, F.; Rugo, H. S.; Mayer, I. A.; et al. Gedatolisib in Combination Therapy for Hormone Receptor-Positive, HER2-Negative Advanced Breast Cancer: Clinical Evaluation and Therapeutic Potential. Clin. Cancer Res. 2023, 29, 1502–1510.
26. Arun M. Venkatesan; Christopher M. Dehnhardt; Eduardo Delos Santos; Zheng Chen; Osvaldo Dos

Santos; Silvina Ayral-Kaloustian; Gulnara Khafizova; Nico Brooijmans; Richard Mallon; Irwin Hollander; Leonard Feldberg; James Lucas; Kathy Yu; Joseph Gibbons; Richard T. Abraham; Inder Chaudhary; Tarek S. Mansour. Bis(morpholino-1,3,5-triazine) Derivatives: Potent Adenosine 5′-Triphosphate Competitive Phosphatidylinositol-3-Kinase/Mammalian Target of Rapamycin Inhibitors. Discovery of Compound 26 (PKI-587), a Highly Efficacious Dual Inhibitor. Journal of Medicinal Chemistry 2010, 53 (6), 2636–2645.

27. Michael Shields; Qing Mo; Matthew Armitage; Stephen C. Sharpe; Ricardo L. B. A. Costa. A Systematic Review and Meta-Analysis of Selected Toxicity Endpoints of Alpelisib. Oncotarget 2020, 11 (42), 3793–3799.
28. Yunlong Zhao; Xiaofeng Zhang; Yong Chen; Shuang Lu; Yujie Peng; Xin Wang; Cheng Guo; Aimin Zhou; Jing Zhang; Yong Luo; Qin Shen; Jingkang Ding; Lingyi Meng; Jin Zhang. Crystal Structures of PI3Kα Complexed with PI-103 and Its Derivatives: New Directions for Inhibitor Design. ACS Medicinal Chemistry Letters 2014, 5 (2), 138–142.
29. Jean A. Engelman. Targeting PI3K Signalling in Cancer: Opportunities, Challenges and Limitations. Nature Reviews Cancer 2009, 9, 550–562.
30. Bart Vanhaesebroeck; Laurent Guillermet-Guibert; Maria Graupera; Bilal Bilanges. The Emerging Mechanisms of Isoform-Specific PI3K Signalling. Nature Reviews Molecular Cell Biology 2010, 11, 329–341.
31. Lewis C. Cantley. The Phosphoinositide 3-Kinase Pathway. Science 2002, 296, 1655–1657.
32. David A. Fruman; Benjamin D. Hopkins; Benedikt B. Rommel. The PI3K Pathway in Human Disease. Cell 2017, 170, 605–635.
33. Fabrice Andre; Hope S. Rugo; Stefan Loibl; et al. Alpelisib for PIK3CA-Mutated, Hormone Receptor–Positive Advanced Breast Cancer. New England Journal of Medicine 2019, 380, 1929–1940.
34. Michael Shields; Qing Mo; Matthew Armitage; Stephen C. Sharpe; Ricardo L. B. A. Costa. A Systematic Review and Meta-Analysis of Selected Toxicity Endpoints of Alpelisib. Oncotarget 2020, 11 (42), 3793–3799.
35. Yunlong Zhao; Xiaofeng Zhang; Yong Chen; et al. Crystal Structures of PI3Kα Complexed with PI-103 and Its Derivatives: New Directions for Inhibitor Design. ACS Medicinal Chemistry Letters 2014, 5 (2), 138–142.
36. Paul Workman; Paul Clarke. Kinase Inhibitors: Opportunities and Challenges in Drug Discovery. Nature Reviews Drug Discovery 2011, 10, 307–322.
37. Benjamin D. Hopkins; Jason M. Goncalves; Lewis C. Cantley. Insulin-PI3K Signalling in Cancer. Nature Reviews Drug Discovery 2018, 17, 627–644.
38. Jean A. Engelman; Jarrod A. Martelli. Targeting the PI3K Pathway in Cancer Therapy. Nature Reviews Clinical Oncology 2013, 10, 575–585.
39. Marco Falasca; Marco Maffucci. Role of Phosphoinositide 3-Kinase in Cancer. Current Medicinal Chemistry 2012, 19, 173–183.
40. James E. Burke; Roger L. Williams. Structural Mechanisms of PI3K Activation and Inhibition. Nature 2015, 519, 122–126.
41. Klaus Furet; Paul Guagnano. Discovery of NVP-BEZ235, a Dual PI3K/mTOR Inhibitor. Bioorganic & Medicinal Chemistry Letters 2009, 19, 477–480.
42. Matthew A. Lemmon; Joseph Schlessinger. Cell Signaling by Receptor Tyrosine Kinases. Cell 2010, 141, 1117–1134.
43. Kevin M. Courtney; Bradley A. Corcoran; Jonathan A. Engelman. The PI3K Pathway as Drug Target in Human Cancer. Journal of Clinical Oncology 2010, 28, 1075–1083.
44. Benjamin D. Hopkins; Jason M. Goncalves; Lewis C. Cantley. Insulin–PI3K Signaling: An Evolutionarily Insulated Metabolic Driver of Cancer. Nature Reviews Endocrinology 2020, 16, 276–283.
45. Roger L. Williams; Jonathan E. Burke. Structural Basis for Phosphoinositide 3-Kinase Regulation and Inhibition. Science 2012, 337, 134.